Journal of Zhejiang University SCIENCE A
ISSN 1673-565X (Print); ISSN 1862-1775 (Online)
www.zju.edu.cn/jzus; www.springerlink.com
E-mail: jzus@zju.edu.cn

Nonlinear dynamic analysis of the Three Gorge Project powerhouse excited by pressure fluctuation*

Cun-hui ZHANG, Yun-liang ZHANG†‡

(*School of Civil and Hydraulic Engineering, Dalian University of Technology, Dalian 116024, China*)

†E-mail: zhangyl@dl.cn

Received June 22, 2008; Revision accepted Nov. 20, 2008; Crosschecked July 15, 2009

Abstract: This study established a 3D finite element model for 15# hydropower house of the Three Gorges Project (TGP) and performed a nonlinear dynamic analysis under pressure fluctuation. In this numerical model, the stiffness degradation in tension for concrete was considered on the basis of the continuum isotropic damage theory. Natural vibration frequencies of the damaged and undamaged structures were compared after static water pressure was applied. Then a study was further conducted on forced vibration of the powerhouse with pre-existing damages under pressure fluctuation that acts on the flow passage; displacement, velocity and acceleration of the important structural members were afterwards presented and checked. Numerical results show that tensile damages in concrete surrounding the spiral case only exert significant impact upon the dynamic characteristics of sub-structure but show little effect on the superstructure. Nevertheless vibrations of the powerhouse are still under the recommended vibration limits.

Key words: Three Gorges Project (TGP), Hydropower house, Dynamic, Nonlinear, Damage, Pressure fluctuation
doi:10.1631/jzus.A0820478 **Document code:** A **CLC number:** TV3; TV6; TV7; TV22

INTRODUCTION

Intense attention has been given to the vibration of powerhouses of the Three Gorges Project (TGP) ever since the very start of the project. Due to its giant external dimensions and relatively low stiffness, a powerhouse may experience severe vibrations excited by various kinds of dynamic loads. According to the model tests' estimation and evaluation of the vibrations of TGP's left-bank turbine generator sets, the magnitudes of pressure fluctuation were large, surpassing the regulations of the bid document under certain working conditions; this might lead to severe vibrations of the powerhouse and affect the health of staff and normal operations of the hydropower station. It is therefore of great importance to conduct vibration analyses of the powerhouse. Up to now, a number of studies have been made on the vibration analysis of powerhouse structure under pressure fluctuation, but most of them only examined vibrations of small amplitude and assumed concrete materials to be elastic (Shen *et al*., 2003; Ma *et al.*, 2004; Chen *et al.*, 2007).

However, due to high tensile stress resulted from high *HD* (*H* and *D* denote water head and diameter of an inlet pipe, respectively), damages will occur on some locations of concrete surrounding the spiral case and definitely reduce the entire stiffness of the hydropower house, which may bring negative effects on anti-vibration performances of the structure and stable operation of hydro-generator sets (Zhang *et al.*, 2006; 2009; Zhang C.H. *et al.*, 2008). Very few recent studies have been conducted on effects of damage presence on dynamic characteristics of a powerhouse. Jiang *et al.*(2007) created an axial symmetrical finite element model for estimating dynamic characteristics of the powerhouse with damages in the concrete surrounding the spiral case. According to some 3D nonlinear static analyses and laboratory tests (Ma

‡ Corresponding author

* Project (No. 50809013) supported by the National Natural Science Foundation of China

et al., 2006a; 2006b; Su *et al.*, 2006; Wang *et al.*, 2006; Wu H.G. *et al.*, 2006), Zhang Y.L. *et al*.(2008) generalized the distribution of cracks in the concrete surrounding the spiral case and then developed a 3D dynamic analysis model. By supposing two simplified modeling schemes, effects of existing cracks on the dynamic characteristics of a powerhouse were roughly estimated. However, in that work, no consideration had been paid to the propagation and development of cracks and the cracks are always supposed open during the vibrations of a powerhouse. It is thus more reasonable to perform a dynamic analysis based on the concrete damage theory in a unified finite element model.

This study established a 3D unified static and dynamic finite element model for 15# hydropower house of the TGP and performed a nonlinear dynamic analysis under pressure fluctuation. In the model, stiffness degradation in tension for concrete materials was considered; natural vibration frequencies of damaged and undamaged structures were compared after the application of static water pressure. Then, this study further examined the forced vibration of a powerhouse with pre-existing damages under pressure fluctuation that acted on the flow passage. Note that the simulation was performed with the commercial software Abaqus 6.7.

BASIC THEORY

Concrete stress-strain relations

Concrete material features its low tensile strength particularly at low-confining pressures, which results in tensile cracking at a very low stress as compared with compressive stresses. The tensile cracking reduces the stiffness of concrete structural components and therefore, the use of continuum damage mechanics is necessary to accurately model the degradation in the mechanical properties of concrete. However, concrete materials also undergo some irreversible (plastic) deformations in the course of unloading such that the continuum damage theories cannot be used alone, especially at high-confining pressures (Cicekli *et al.*, 2007).

Therefore, the nonlinear behavior of concrete materials can be attributed to two distinct mechanical processes: damage (micro-cracks, micro-cavities, nucleation and coalescence, decohesions, grain boundary cracks, and cleavage in regions of high stress concentration) and plasticity, whose mechanism in concrete has not been completely understood up to date. These two degradation phenomena may be described best by theories of continuum damage mechanics and plasticity. Therefore, a model that accounts for both plasticity and damage is necessary (Lee and Fevens, 1998; Voyiadjis *et al*., 2004; 2008; Wu J.U. *et al*, 2006; Cicekli *et al.*, 2007).

Integrative accounts of plasticity and damage are usually implemented on the basis of isotropic hardening combined with either isotropic (scalar) or anisotropic (tensor) damage. Isotropic damage is widely used due to its simplicity such that different types of combinations with plasticity models have been proposed. One type of such combinations relies on stress-based plasticity formulated in the effective (undamaged) space, where the effective stress is defined as the average micro-scale stress acting on the undamaged material between micro-defects. The other type is based on stress-based plasticity in the nominal (damaged) stress space, where the nominal stress is defined as the macro-scale stress acting on both damaged and undamaged materials (Cicekli *et al.*, 2007). However, it shows that coupled plastic-damage models formulated in the effective space are numerically more stable and attractive (Voyiadjis *et al.*, 2004; 2008; Abaqus Theory Manual, 2007; Cicekli *et al.*, 2007).

In this work, based on the isotropic damage theory, a coupled plastic-damage model formulated in the effective (undamaged) space was adopted as shown in Eq.(1) (Lubliner *et al.*, 1989; Lee and Fevens, 1998; Abaqus Theory Manual, 2007):

$$\boldsymbol{\sigma} = (1-d)\boldsymbol{D}_0^{\mathrm{el}} : (\boldsymbol{\varepsilon} - \boldsymbol{\varepsilon}^{\mathrm{pl}}) = \boldsymbol{D}^{\mathrm{el}} : (\boldsymbol{\varepsilon} - \boldsymbol{\varepsilon}^{\mathrm{pl}}), \quad (1)$$

where $\boldsymbol{\sigma}$ and $\boldsymbol{\varepsilon}$ are Cauchy stress and strain, respectively. An additive strain rate decomposition is assumed:

$$\dot{\boldsymbol{\varepsilon}} = \dot{\boldsymbol{\varepsilon}}^{\mathrm{el}} + \dot{\boldsymbol{\varepsilon}}^{\mathrm{pl}}, \quad (2)$$

where $\dot{\boldsymbol{\varepsilon}}$ is the total strain rate tensor, $\dot{\boldsymbol{\varepsilon}}^{\mathrm{el}}$ and $\dot{\boldsymbol{\varepsilon}}^{\mathrm{pl}}$ are the elastic and plastic parts of $\dot{\boldsymbol{\varepsilon}}$, respectively. $\boldsymbol{D}_0^{\mathrm{el}}$ denotes the initial (undamaged) elastic stiffness of the

material; $\boldsymbol{D}^{\mathrm{el}}=\boldsymbol{D}_0^{\mathrm{el}}(1-d)$ represents the degraded elastic stiffness; and d is the scalar stiffness degradation variable, which can range from 0 (undamaged material) to 1 (fully damaged material). Within the context of the scalar-damage theory, the stiffness degradation, is isotropic and is characterized by a single degradation variable d, which is a function of the stress state and two independent uniaxial damage variables, d_{t} and d_{c}:

$$(1-d)=(1-s_{\mathrm{t}}d_{\mathrm{c}})(1-s_{\mathrm{c}}d_{\mathrm{t}}),\ 0\le s_{\mathrm{t}},s_{\mathrm{c}}\le 1, \tag{3}$$

where d_{t} and d_{c} are increasing functions of the equivalent plastic tension strain $\tilde{\varepsilon}_{\mathrm{t}}^{\mathrm{pl}}$ and the compression strain $\tilde{\varepsilon}_{\mathrm{c}}^{\mathrm{pl}}$:

$$\begin{aligned} d_{\mathrm{t}}&=d_{\mathrm{t}}(\tilde{\varepsilon}_{\mathrm{t}}^{\mathrm{pl}},f_i),\ 0\le d_{\mathrm{t}}\le 1,\\ d_{\mathrm{c}}&=d_{\mathrm{c}}(\tilde{\varepsilon}_{\mathrm{c}}^{\mathrm{pl}},f_i),\ 0\le d_{\mathrm{c}}\le 1, \end{aligned} \tag{4}$$

where f_i (i=1, 2, 3, …) are the predefined field variables. Response of concrete to uniaxial loading in tension and compression is described by Fig.1, where σ_{t}, σ_{c}, ε_{t}, ε_{c} are concrete tensile stress, compressive stress, tensile strain and compressive strain

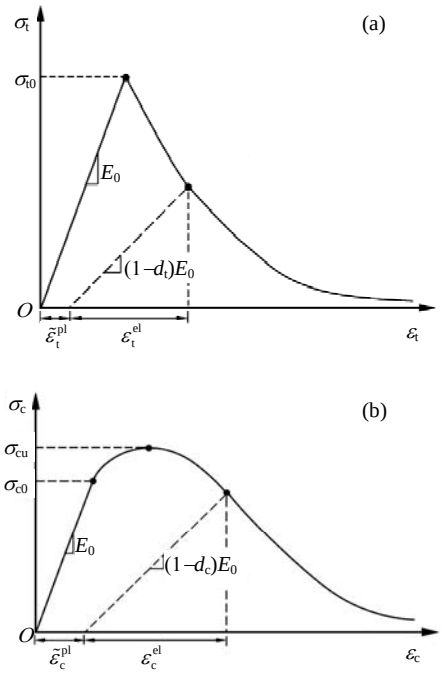

Fig.1 Response of concrete to uniaxial loading in (a) tension and (b) compression

respectively in uniaxial loading case; E_0 is the initial concrete elastic modulus.

The evolution of d is governed by the equivalent plastic strain $\tilde{\boldsymbol{\varepsilon}}^{\mathrm{pl}}=[\tilde{\varepsilon}_{\mathrm{t}}^{\mathrm{pl}},\tilde{\varepsilon}_{\mathrm{c}}^{\mathrm{pl}}]$ and the effective stress $\bar{\boldsymbol{\sigma}}$; that is, $d=d(\bar{\boldsymbol{\sigma}},\tilde{\boldsymbol{\varepsilon}}^{\mathrm{pl}})$, where the subscripts t and c refer to tension and compression, respectively. The equivalent plastic strains $\tilde{\boldsymbol{\varepsilon}}^{\mathrm{pl}}=[\tilde{\varepsilon}_{\mathrm{t}}^{\mathrm{pl}},\tilde{\varepsilon}_{\mathrm{c}}^{\mathrm{pl}}]$ can be obtained through the integration of equivalent plastic strain rates $\dot{\tilde{\varepsilon}}_{\mathrm{t}}^{\mathrm{pl}}$, $\dot{\tilde{\varepsilon}}_{\mathrm{c}}^{\mathrm{pl}}$ with respect to time t:

$$\tilde{\varepsilon}_{\mathrm{t}}^{\mathrm{pl}}=\int_0^t\dot{\tilde{\varepsilon}}_{\mathrm{t}}^{\mathrm{pl}}\mathrm{d}t,\quad \tilde{\varepsilon}_{\mathrm{c}}^{\mathrm{pl}}=\int_0^t\dot{\tilde{\varepsilon}}_{\mathrm{c}}^{\mathrm{pl}}\mathrm{d}t. \tag{5}$$

As for the equivalent plastic strain rates, they can be evaluated as follows:

$$\dot{\tilde{\varepsilon}}_{\mathrm{t}}^{\mathrm{pl}}=r(\hat{\bar{\boldsymbol{\sigma}}})\dot{\hat{\varepsilon}}_{\max}^{\mathrm{pl}},\ \dot{\tilde{\varepsilon}}_{\mathrm{c}}^{\mathrm{pl}}=-(1-r(\hat{\bar{\boldsymbol{\sigma}}}))\dot{\hat{\varepsilon}}_{\min}^{\mathrm{pl}}, \tag{6}$$

where $\dot{\hat{\varepsilon}}_{\max}^{\mathrm{pl}}$ and $\dot{\hat{\varepsilon}}_{\min}^{\mathrm{pl}}$ are, respectively, the maximum and minimum eigenvalues of the plastic strain rate tensor $\dot{\boldsymbol{\varepsilon}}^{\mathrm{pl}}$ and

$$r(\hat{\bar{\boldsymbol{\sigma}}})=\sum_{i=1}^{3}\langle\bar{\sigma}_i\rangle\Big/\sum_{i=1}^{3}|\bar{\sigma}_i|,\quad 0\le r(\hat{\bar{\boldsymbol{\sigma}}})\le 1, \tag{7}$$

where $r(\hat{\bar{\boldsymbol{\sigma}}})$ is a stress weight factor that is equal to 1 if all principal stresses $\hat{\bar{\sigma}}_i$ (i=1, 2, 3) are positive, and equal to 0 if they are negative. The Macauley bracket $\langle\cdot\rangle$ is defined by $\langle x\rangle=(|x|+x)/2$. If the eigenvalues of the plastic strain rate tensor ($\dot{\hat{\varepsilon}}_i$, i=1, 2, 3) are ordered such that $\dot{\hat{\varepsilon}}_{\max}^{\mathrm{pl}}=\dot{\hat{\varepsilon}}_1\ge\dot{\hat{\varepsilon}}_2\ge\dot{\hat{\varepsilon}}_3=\dot{\hat{\varepsilon}}_{\min}^{\mathrm{pl}}$, the evolution equation for multiaxial stress conditions can be expressed as follows:

$$\dot{\tilde{\boldsymbol{\varepsilon}}}^{\mathrm{pl}}=[\dot{\tilde{\varepsilon}}_{\mathrm{t}}^{\mathrm{pl}},\dot{\tilde{\varepsilon}}_{\mathrm{c}}^{\mathrm{pl}}]=[r(\hat{\bar{\boldsymbol{\sigma}}})\dot{\hat{\varepsilon}}_1,-(1-r(\hat{\bar{\boldsymbol{\sigma}}}))\dot{\hat{\varepsilon}}_3]. \tag{8}$$

Effective stress tensor $\bar{\boldsymbol{\sigma}}$ is defined by

$$\bar{\boldsymbol{\sigma}}=\boldsymbol{D}_0^{\mathrm{el}}:(\boldsymbol{\varepsilon}-\boldsymbol{\varepsilon}^{\mathrm{pl}}), \tag{9}$$

therefore, the relationship between Cauchy stress and effective stress is obtained via

$$\boldsymbol{\sigma}=(1-d)\bar{\boldsymbol{\sigma}}. \tag{10}$$

In Eq.(3) s_t and s_c are functions of the stress state that are defined by

$$\begin{aligned} s_t &= 1-w_t\cdot r(\hat{\bar{\boldsymbol{\sigma}}}),\quad 0\le w_t\le 1,\\ s_c &= 1-w_c\cdot(1-r(\hat{\bar{\boldsymbol{\sigma}}})),\ 0\le w_c\le 1, \end{aligned} \tag{11}$$

where $\hat{\bar{\sigma}}_i$ is the principal component of effective stress tensor $\bar{\boldsymbol{\sigma}}$; the weight factors w_t and w_c are assumed to be material properties and to control the recovery of the tensile and compressive stiffness upon load reversal. The experimental observation in most quasi-brittle materials, including concrete, is that the compressive stiffness is recovered upon closure as the load changes from tension to compression. On the other hand, the tensile stiffness is not recovered as the load changes from compression to tension once crushing micro-cracks have developed. This behavior corresponds to w_c=1 and w_t=0.

Yield condition

The plastic-damage concrete model uses a yield condition on the basis of the yield function devised by Lubliner *et al*.(1989) and incorporates the modifications proposed by Lee and Fenves (1998) to account for different evolutions of strength under tension and compression. In terms of effective stresses the yield function takes the form of

$$\begin{aligned} F(\bar{\boldsymbol{\sigma}},\tilde{\boldsymbol{\varepsilon}}^{\mathrm{pl}}) = \frac{1}{1-\alpha}(\bar{q}-3\alpha\bar{p}+\beta(\tilde{\boldsymbol{\varepsilon}}^{\mathrm{pl}})\langle\hat{\bar{\sigma}}_{\max}\rangle\\ -\gamma\langle-\hat{\bar{\sigma}}_{\max}\rangle)-\bar{\sigma}_c(\tilde{\varepsilon}_c^{\mathrm{pl}})\le 0, \end{aligned} \tag{12}$$

where α and γ are dimensionless material constants. Typical experimental values of α are within 0.08 to 0.12 (Lubliner *et al.*, 1989). The coefficient γ enters the yield function only for stress states of triaxial compression when $\hat{\bar{\sigma}}_{\max}$ <0. $\hat{\bar{\sigma}}_{\max}$ is the algebraically maximum eigenvalue of the effective stress tensor $\bar{\boldsymbol{\sigma}}$. A typical value for concrete gives γ=3. $\bar{p}=-\frac{1}{3}\bar{\boldsymbol{\sigma}}:\boldsymbol{I}$ is the effective hydrostatic pressure; $\bar{q}=\sqrt{\frac{3}{2}\bar{\boldsymbol{S}}:\bar{\boldsymbol{S}}}$ represents the von Mises equivalent effective stress; $\bar{\boldsymbol{S}}=\bar{p}\boldsymbol{I}+\bar{\boldsymbol{\sigma}}$ refers to the deviatoric part of $\bar{\boldsymbol{\sigma}}$. The function $\beta(\tilde{\boldsymbol{\varepsilon}}^{\mathrm{pl}})$ is presented as

$$\beta(\tilde{\boldsymbol{\varepsilon}}^{\mathrm{pl}})=\frac{\bar{\sigma}_c(\tilde{\varepsilon}_c^{\mathrm{pl}})}{\bar{\sigma}_t(\tilde{\varepsilon}_t^{\mathrm{pl}})}(1-\alpha)-(1+\alpha), \tag{13}$$

where $\bar{\sigma}_t$ and $\bar{\sigma}_c$ denote the effective tensile and compressive cohesion stresses, respectively.

Flow rule

The plastic-damage model assumes a non-associated potential flow rule and the flow potential G chosen for this model is the Drucker-Prager hyperbolic function:

$$\dot{\boldsymbol{\varepsilon}}^{\mathrm{pl}}=\dot{\lambda}\frac{\partial G(\bar{\boldsymbol{\sigma}})}{\partial\bar{\boldsymbol{\sigma}}}, \tag{14}$$

$$G=\sqrt{(\text{ə}\,\sigma_{t0}\tan\psi)^2+\bar{q}^2}-\bar{p}\tan\psi, \tag{15}$$

$$\dot{\lambda}\cdot\dot{F}(\bar{\boldsymbol{\sigma}},\tilde{\boldsymbol{\varepsilon}}^{\mathrm{pl}})=0,\ \dot{\lambda}\ge 0,\ F(\bar{\boldsymbol{\sigma}},\tilde{\boldsymbol{\varepsilon}}^{\mathrm{pl}})\le 0, \tag{16}$$

where $\dot{\lambda}$ is the nonnegative plastic multiplier that should obey the Kuhn-Tucker and consistency conditions as described by Eq.(16). ψ denotes the dilation angle measured in the $\bar{p}$ - $\bar{q}$ plane; σ_{t0} refers to the uniaxial tensile stress at failure; and ə represents a parameter that is referred to as the eccentricity and defines the rate at which the function approaches the asymptote (the flow potential is likely to form a straight line as the eccentricity approaches zero).

SPECIAL CONSIDERATION

Before the tensile stress of the concrete reaches the tensile strength σ_{t0}, the curve is linear and the material remains elastic. In this study, only the degradation of the elastic stiffness in tension was considered; it is based on the fact that the tensile stress of concrete surrounding the spiral case often surpasses the strength σ_{t0} while the compressive stress often become less than the elastic compressive strength σ_{c0}. This means $d_t\neq 0$, d_c=0. Hence, simplifications can be made in Eqs.(1)~(16). According to (GB50010-2002, 2002), after the tensile stress reaches σ_{t0}, the curve is nonlinear in the form of

$$y=\frac{x}{\alpha_t(x-1)^{1.7}+x}, \tag{18}$$

where $x=\varepsilon_t/\varepsilon_{t0}$ and $y=\sigma_t/\sigma_{t0}$, which are dimensionless strain and stress, respectively. ε_{t0} refers to the strain corresponding to σ_{t0}; σ_t and ε_t are the stress and strain at a point on the strain softening branch of the stress-strain curves, respectively. α_t is the coefficient that is determined by

$$\alpha_t=0.312\sigma_{t0}. \tag{19}$$

For C25 concrete, the post-failure stress σ_t is a function of cracking strain ε_t^{ck} (Fig.2). Herein ε_t^{ck} is defined as (Fig.3)

$$\varepsilon_t^{ck}=\varepsilon_t-\varepsilon_{t0}^{el}, \tag{20}$$

$$\varepsilon_{t0}^{el}=\sigma_t/E_0, \tag{21}$$

The equivalent plastic strain ε_t^{pl} is proposed by Yankelevsky (1987) with

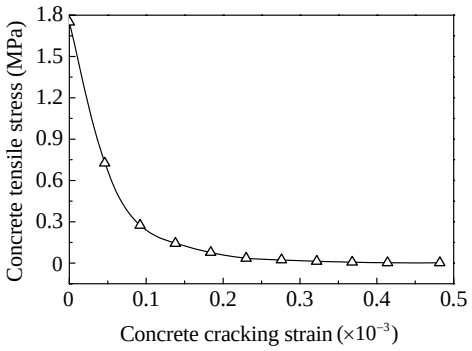

Fig.2 Concrete tensile stress σ_t vs cracking strain ε_t^{ck}

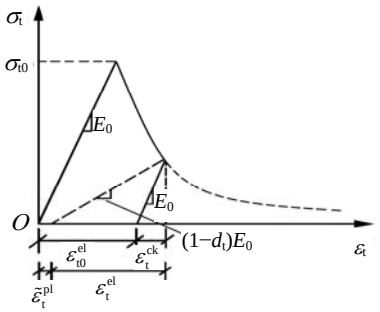

Fig.3 Illustration of the definition of the cracking strain ε_t^{ck}

$$\varepsilon_t^{pl}=(\sigma_{t0}\varepsilon_t-\sigma_t\sigma_{t0}/E_0)/(\sigma_t+\sigma_{t0}). \tag{22}$$

Then damage variable d_t is computed by

$$\sigma_t=(1-d_t)E_0(\varepsilon_t-\varepsilon_t^{pl}). \tag{23}$$

In this study, the d_t-ε_t^{ck} curve adopted is shown in Fig.4.

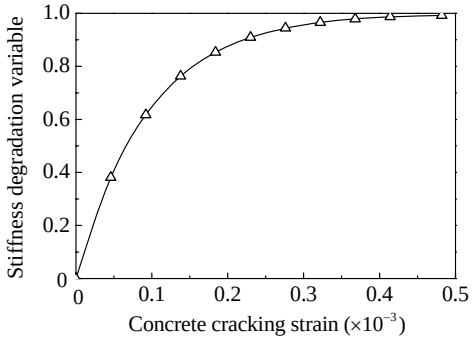

Fig.4 Relation between stiffness degradation in tension with cracking strain ε_t^{ck}

Mesh-dependency often occurs for pure concrete structures, while in this work six layers of rebars (very closely distributed) are designed and arranged for concrete surrounding the spiral case (Fig.5). For reinforced concrete structures, the effect of mesh-dependency is minor due to interactions of rebars with concrete. Furthermore, in the procedure of numerical implementation, a viscoplastic regularization method is proposed by Lee and Fevens (1998) based on the Duvaut-Lions model not only to make the system well-posed, but also to help eliminate the mesh-dependency. On the other hand, in this study only concrete surrounding the spiral case was assumed to be nonlinear in material properties due to computation cost and research aim limits. Concrete of other parts of the powerhouse still remains elastic and linear. Accordingly, the dynamic response of the entire powerhouse is almost not influenced by the mesh-dependency. A more effective and general way to void mesh-dependency is to adopt σ_t-δ_t curve, where δ_t is the cracking displacement, in place of σ_t-ε_t curve as pointed out by Hilleborg (1976). In this study, due to lack of test data for C25 concrete under tension and compression to get the curve σ_t-δ_t, the σ_t-ε_t curve was therefore chosen and applied according to (GB50010-2002, 2002).

NUMERICAL MODEL

We established a unified finite element model for analyzing the static and dynamic responses of the powerhouse, which includes super and sub-structure as well as bed rocks (Fig.6). Fig.7 presents the meshes of rebars embedded into concrete that are at the first layer near the steel liner respectively in and perpendicular to water flow directions. The arrangement of rebars for concrete surrounding the spiral case is shown in detail in Fig.5, where the unit is m for elevation and size for concrete, while mm for rebar arrangement.

In the global coordinate system of the model, *Z*-axis is horizontal with the positive direction moving from downstream towards upstream, and *Y*-axis is vertical with the positive direction moving upward. *X*-axis is horizontal, specifically perpendicular to *Z*-axis.

In the model, the reinforcement element is embedded directly into the concrete element and the nodal degree of freedom is coupled automatically by assuming that there is no relative slippage between the reinforcement and concrete elements.

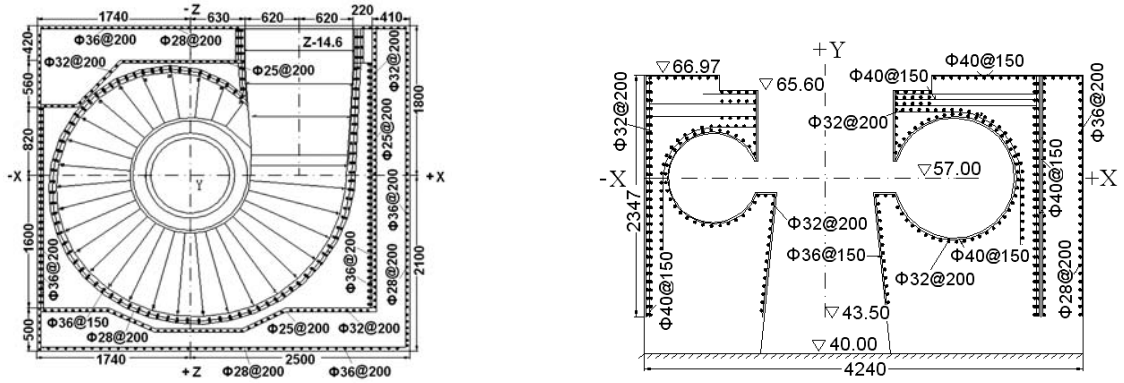

(a) (b)

Fig.5 Plane view (a) and vertical view (b) of rebars for concrete surrounding the spiral case

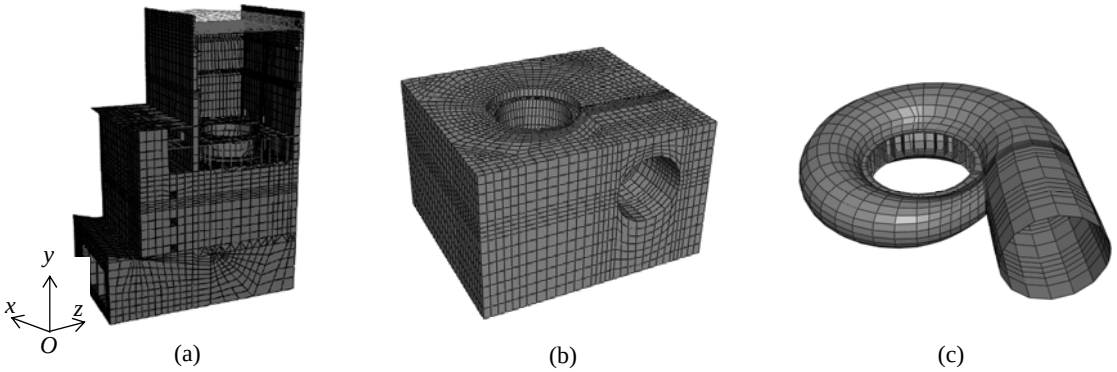

(a) (b) (c)

Fig.6 Finite element meshes for (a) 15# powerhouse of the TGP (bedrocks not plotted); (b) concrete; (c) spiral case

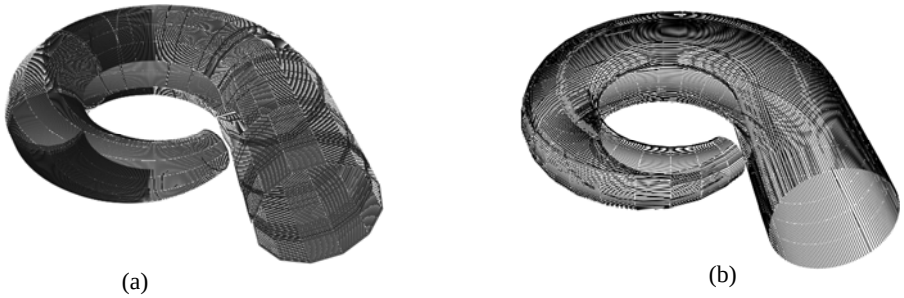

(a) (b)

Fig.7 Finite element meshes for (a) rebars perpendicular to water flow direction and (b) rebars in water flow direction, which are at the first layer near the steel liner

MATERIAL PARAMETERS

In this study, the plastic-damage model for concrete surrounding the spiral case was adopted. The isotropic elastic-plastic model that satisfies the von Mises yield criterion was used for steel materials in the numerical model. Some elastic parameters adopted in this study are listed in Table 1.

Table 1 Parameters for steel and concrete material

Material	Density (kN/m^3)	Yong's modulus (GPa)	Poisson's ratio	Compressive strength (MPa)	Tensile strength (MPa)
Concrete (C25)	25.0	28.0	0.167	17.0	1.75
Steel plate	78.5	210	0.3	370	370
Stator ring (Q235B)	78.5	210	0.3	205	205
Rebar (Grade II)	78.5	210	0.3	310	310

LOADS AND LOAD STEPS

All static and dynamic loads related were applied according to the following steps. Load step 1, the loads such as the self-weight and live loads on the floor slabs are applied, and notably, no water is charged in spiral case and draft tube. Load step 2, apply the loads such as the internal water pressure (including static hydro-pressure plus dynamic pressure fluctuation), and the water thrust that is transferred from the top-cover of hydraulic turbines to annular plates of the stay ring. At the second load step, the water is charged, the generator set is in normal operation and notably, the loads in the first step remain.

Pressure fluctuation at nine measuring points that are distributed near the turbine head cover, inside wall of the steel spiral case and the draft tube was provided by model tests. In normal operation cases, typical time histories of the pressure fluctuation acting on the wall of the spiral case and the draft tube are shown in Fig.8. It can be seen that the amplitude of pressure fluctuation is just about 1%~4% of that of the static pressure. In the calculation, the Hibller-Hughes-Taylor time integration scheme was adopted with the maximum time interval of 0.0225 s, and the Rayleigh damping matrix with the constant modal damping ratio of 5% was assumed.

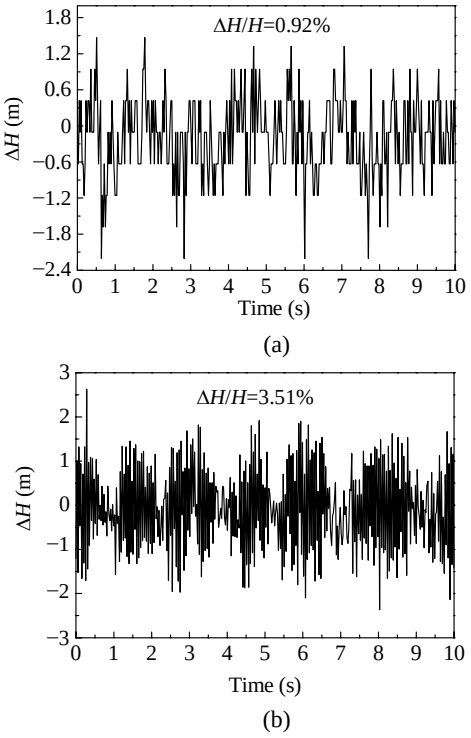

Fig.8 Typical time history of the pressure pulsation acting on (a) the spiral case and (b) the draft tube

RESULTS AND ANALYSES

Damage analysis

Distributions of tensile damage in concrete surrounding the spiral case after Load step 2 are shown in Fig.9.

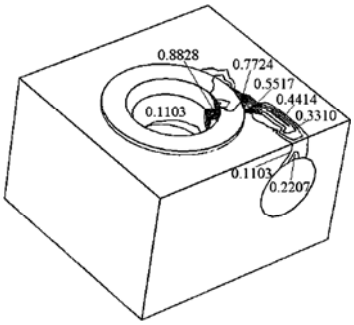

Fig.9 Damage distributions in concrete surrounding the spiral case under static hydro-pressure plus pressure fluctuation

It can be seen from Fig.9 that after Load step 2, plastic deformation and damage occur in the concrete surrounding the spiral case with the maximum of damage variable d_t of up to 0.8828. The damages

were mainly located near the top of the inlet section of the spiral case.

Frequency comparison for damaged and undamaged structures

To explore effects of damage presence on natural frequencies of the powerhouse, two numerical models were adopted. Model I designates the undamaged structure that remains linear and elastic under external forces, and Model II aims to simulate the damaged structure; i.e., the powerhouse was under the action of external forces as mentioned above in Load steps 1~2 based on the concrete plastic damage theory.

The first 50 natural frequencies of the powerhouse for Models I and II are given in Table 2.

From Table 2, it can be concluded that the natural vibration frequencies of the same order in Model II are very close to those in Model I. The maximum of frequency reduction percentage is only 0.112% at order 23, indicating that damages in concrete surrounding the spiral case have no great effect on the natural frequencies of the powerhouse.

Vibration responses under pressure fluctuation

Maximum dynamic responses of the upstream and downstream walls, the stator foundation and the lower bracket foundation under the action of fluctuating pressure are listed in Table 3. Given the commonly severe vibration of floor slabs, 12 points (Fig.10) on the generator floor slab were selected to check the vibration level. Vibration displacement, velocity, and acceleration of the floor slab are given in Table 4; in addition, Fig.11 presents distributions of vertical displacements of upstream and downstream walls along the height.

Table 2 The first 50 natural frequencies of powerhouse (Hz)

Order	Frequency (Hz)		Reduction percentage (%)
	Model I	Model II	
1	0.8595	0.8594	0.012
2	1.1549	1.1548	0.009
3	1.5907	1.5907	0
4	6.030	6.029	0
…	…	…	…
22	6.251	6.244	0.017
23	6.452	6.451	0.112
24	9.0682	9.0681	0.016
…	…	…	…
48	9.432	9.431	0.001
49	9.520	9.519	0.011
50	4.0261	4.0257	0.011

Table 3 Vibration responses of foundation and wall

Location	Displacements (mm)			Velocity (mm/s)			Acceleration (m/s^2)		
	u_x	u_y	u_z	v_x	v_y	v_z	a_x	a_y	a_z
Stator foundation	0.0248	0.170	0.159	0.972	2.73	1.172	0.263	0.738	0.267
Lower bracket foundation	0.0215	0.176	0.136	0.702	2.57	1.007	0.299	0.672	0.141
Upstream wall	0.1020	0.388	0.187	2.394	8.07	7.270	0.212	0.396	0.877
Downstream wall	0.1080	0.393	0.169	1.159	6.11	2.190	0.150	0.354	0.778

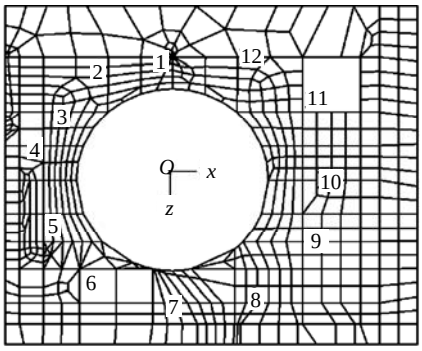

Fig.10 Selected points on the slab at a generator floor

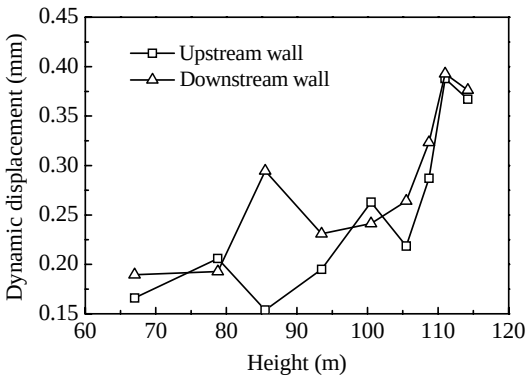

Fig.11 Vertical displacement distributions of upstream and downstream walls along height

Table 4 Vibration responses of the generator floor slab

Point	Displacements (mm)			Velocity (mm/s)			Acceleration (m/s^2)		
	u_x	u_y	u_z	v_x	v_y	v_z	a_x	a_y	a_z
1	0.0284	0.258	0.147	0.150	1.093	1.612	0.0155	0.250	0.0287
2	0.0338	0.278	0.211	0.160	0.876	1.484	0.0208	0.172	0.0288
3	0.0317	0.345	0.135	0.190	0.844	1.411	0.0258	0.137	0.0309
4	0.0162	0.318	0.132	0.212	0.787	1.400	0.0270	0.128	0.0316
5	0.0145	0.291	0.129	0.283	0.738	1.358	0.0260	0.126	0.0337
6	0.0329	0.272	0.125	0.483	0.641	1.339	0.0251	0.108	0.0342
7	0.0225	0.188	0.127	0.576	0.569	1.427	0.0277	0.113	0.0323
8	0.0004	0.222	0.142	0.596	0.872	1.657	0.0259	0.155	0.0355
9	0.0154	0.326	0.153	0.504	0.836	1.728	0.0191	0.138	0.0326
10	0.0209	0.311	0.162	0.353	0.656	1.765	0.0253	0.105	0.0292
11	0.0068	0.372	0.163	0.208	0.837	1.714	0.0158	0.142	0.0302
12	0.0152	0.260	0.156	0.149	0.998	1.707	0.0104	0.216	0.0294

In the past decades, there are a large number of reports and studies on vibration estimation and control of units and powerhouses. After summarizing some vibration control standards for human health, building, equipment and apparatus, Ma and Dong (2004) suggested the vibration response limits for the TGP powerhouses (Table 5).

Table 5 Suggested vibration response limits for the TGP powerhouse (Ma and Dong, 2004)

Structural member	Displacements (mm)	Velocity (mm/s)	Acceleration (m/s^2)
Floor slab	0.2	5.0	1.0
Solid wall	0.2	10.0	1.0
Concrete surrounding the spiral case	0.2	5.0	1.0

However, it can be seen from Tables 3 and 4, and Fig.11 that the amplitudes of all vibration velocity and acceleration for the powerhouse are less than the suggested limits of Table 5. As for vertical vibration displacement of the generator floor slab and, the upstream and downstream walls, the maximum amplitude exceeds the suggested limit of 0.2 mm. In particular, the maximum displacement in the generator floor slab reaches 0.372 mm (located at the edge of opening in the slab), and the maximum displacements for the upstream and downstream walls amount to 0.393 mm and 0.388 mm, respectively (located on the top of the walls).

Note that dynamic responses in this study based on the damage theory, including vibration displacement, velocity and acceleration, are greater in amplitudes than those based on the linear, elasticity theory presented by (Shen *et al.*, 2003; Chen *et al*., 2007; Ma and Dong, 2004; Zhang Y.L. *et al*., 2008).

CONCLUSION

At the stages of design, manufacture and management for the TGP, the normal and safe operation of the turbine and powerhouse is always a key issue. Due to the induced lower stiffness by the giant *HD* value and adverse operation conditions, dynamic performances of the powerhouse structure were studied through numerical simulations. However, very little public literature has been found on estimation of damage presence in concrete surrounding the spiral case on dynamic performances of the powerhouse.

As the numerical results shown, damages in concrete surrounding the spiral case—from the viewpoint of effects on natural frequencies of the powerhouse—cause no big difference compared to the case that the entire powerhouse is undamaged. However, from the viewpoint of effects on the dynamic responses of the powerhouse under pressure fluctuation, these damages magnify the vibration amplitudes of the powerhouse, especially of its superstructure, such as the generator floor slab, upstream and downstream walls. Presence of the damages makes the vibration displacements on generator floor slab, upstream and

downstream walls, exceed the suggested limits.

However, this work is under the frame of isotropic damage coupled with plasticity for concrete. As well-documented in literature, more realistic simulations are to apply the anisotropic damage-plasticity theory to dynamic analysis.

During its long-term service life, the concrete surrounding the spiral case is loaded and unloaded repeatedly by water, which will cause further evolutions of damage in the concrete. Effects of the final state of damages on structural strength and stiffness after the repeated water pressure had been evaluated by Zhang C.H. *et al.*(2008), which is, however, beyond the scope of this study.

References

Abaqus Theory Manual (Version 6.7), 2007. Dassault Systèmes Inc.

Chen, J., Zhang, Y.L., Ma, Z.Y., Cheng, G.R., Wang, Y., 2007. Study of dynamic characteristics of a giant spiral case with different embedment manners. *Journal of Dalian University of Technology*, **47**(4):593-597 (in Chinese).

Cicekli, U., Voyiadjis, G.Z., Rashid, K., 2007. A plasticity and anisotropic damage model for plain concrete. *International Journal of Plasticity*, **23**:1874-1900.

GB 50010-2002, 2002. Code for Design of Concrete Structures. Ministry of Construction, P. R. China (in Chinese).

Hillerborg, A., Modeer, M., Petersson, P.E., 1976. Analysis of crack formation and crack growth in concrete by means of fracture mechanics and finite elements. *Cement and Concrete Research*, **6**:773-782.

Jiang, K.C., Wu, H.G., Shen, Y., 2007. Nonlinear dynamic responses of complete bearing spiral case under the action of pulsation pressure. *Journal of Hydroelectric Engineering*, **26**(4):104-109 (in Chinese).

Lee, J., Fenves, G.L., 1998. Plastic-damage model for cyclic loading of concrete structures. *Journal of Engineering Mechanics*, **124**(8):892-900.

Lubliner, J., Oliver, J., Oller, S., 1989. A plastic-damage model for concrete. *International Journal of Solids and Structures*, **25**(3):229-326.

Ma, Z.Y., Dong, Y.X., 2004. Vibration and Its Corrective Action of Water Turbine Generator Set and Power House. China Water Resources and Hydropower Publishing House, Beijing (in Chinese).

Ma, Z.Y., Zhang, Y.L., Chen, J., Cheng, G.R., Wang, Y., 2006a. The feasibility evaluation of the giant spiral case using cushion layer. *Water Power*, **32**(1):28-32, 56 (in Chinese).

Ma, Z.Y., Zhang, Y.L., Chen, J., 2006b. Static and Dynamic Analysis Report on Spiral Case Embedded Directly in Concrete for Three Gorge Project's Right Bank Powerstation. Research Report, Dalian University of Technology, Dalian (in Chinese).

Shen, K., Zhang, Z.Q., Liang, Z., 2003. Hydraulic vibration calculation of Yan-tan hydropower house. *Hydroelectric Energy*, **21**(1):72-75 (in Chinese).

Su, H.D., Lin, S.Z., Chen, Q., 2006. Nonlinear Analysis of Spiral Case Embedded Directly in Concrete for Three Gorge Project's Right Bank Powerstation. Research Report, Changjiang River Scientific Research Institute, Wuhan (in Chinese).

Voyiadjis, Z.V., Al-Rub, R.K.A., Palazotto, K.R., 2004. Thermodynamic framework for coupling of non-local viscoplasticity and non-local anisotropic viscodamage for dynamic localization problems using gradient theory. *International Journal of Plasticity*, **20**:981-1038.

Voyiadjis, G.Z., Taqieddin, Z.N., Peter, I.K., 2008. Anisotropic damage-plasticity model for concrete. *International Journal of Plasticity*, **24**(10):1946-1965.

Wang, J.W., 2006. Reinforcement Research on Spiral Case Embedded Directly in Concrete for Three Gorge Project's Right Bank Powerstation. Research Report, Hehai University, Nanjing (in Chinese).

Wu, J.U., Li, J., Faria, R., 2006. An energy release rate-based plastic-damage model for concrete. *International Journal of Solids and Structures*, **43**:583-612.

Wu, H.G., Jiang, K.C., Shen, Y., 2006. Research on Spiral Case Embedded Directly in Concrete for Three Gorge Project's Right Bank Powerstation. Research Report, Wuhan University, Wuhan (in Chinese).

Yankelevsky, D.Z., Reinhardt, H.W., 1989. Uniaxial cyclic behaviour of concrete in tension. *ASCE*, **115**(SEI): 169-176.

Zhang, C.H., Zhang, Y.L., Ma, Z.Y., 2008. Damage analysis of reinforced concrete surrounding the spiral case under repeated water pressure. *Journal of Hydraulic Engineering*, **39**(11):1262-1264 (in Chinese).

Zhang, Y.L., Ma, Z.Y., Cheng, G.R., Chen, J., Wang, Y., 2006. Strength and stiffness analysis of spiral casing with different embedded manners. *Journal of Hydraulic Engineering*, **37**(10):1206-1211 (in Chinese).

Zhang, Y.L., Ma, Z.Y., Wang, Y., Chen, J., 2008. Effect of cracks on dynamic characteristics of hydropower house. *Journal of Hydraulic Engineering*, **39**(8):982-987 (in Chinese).

Zhang, Y.L., Zhang, C.H., Ma, Z.Y., 2009. Nonlinear analysis on a large-scale spiral case directly embedded into concrete. *Journal of Hydraulic Engineering*, **40**(2):220-225 (in Chinese).